Composition dependence of topological and chemical orders in liquid $Al_{1-x}(Mn_y(FeCr)_{1-y})_x$ alloys by neutron diffraction

1991 J. Phys.: Condens. Matter 3 2801

(http://iopscience.iop.org/0953-8984/3/16/019)

J. Phys.: Condens. Matter 3 (1991) 2801–2817. Printed in the UK

Composition dependence of topological and chemical orders in liquid $Al_{1-x}(Mn_y(FeCr)_{1-y})_x$ alloys by neutron diffraction

M Maret†, P Chieux‡, J M Dubois§ and A Pasturel†

† Laboratoire de Thermodynamique et Physico-Chimie Métallurgiques, CNRS Unité Associé 29, ENSEEG, BP 75, 38402 Saint Martin d'Hères Cédex, France

‡ Institut Laue Langevin, BP 156X, 38402 Grenoble Cédex, France

§ Laboratoire de Sciences et Génie des Matériaux Métalliques, CNRS Unité Associé 159, Ecole des Mines, Parc de Saurupt, 54042 Nancy Cédex, France

Received 5 September 1990, in final form 30 January 1991

Abstract. The composition dependence of the topological order in liquid $Al_{1-x}M_x$ (M = Mn or FeCr) alloys was studied by measuring the neutron structure factors of alloys $Al_{1-x}(Mn_{0.304}(FeCr)_{0.696})_x$ (x = 0.14, 0.2, 0.267 and 0.4). The composition of the 3d metal mixture was chosen in such a way that its average coherent scattering length was equal to that of Al atoms, so that the S_{NN} function was directly available from experiment. Important clues indicating a local icosahedral order have been found in the four liquid alloys. Three other neutron diffraction measurements have been performed with the 40 at.% Al liquid alloy with different Mn to σ-FeCr atomic ratios, yielding an accurate determination of the three partial pair-correlation functions. The comparison between the local structures of $Al_{80}M_{20}$ and $Al_{60}M_{40}$ has shown that the strength of heteroatomic interactions is similar in both alloys, while the first MM and AlAl distances are significantly shorter in $Al_{60}M_{40}$.

1. Introduction

The discovery of quasicrystalline phases in AlMn alloys (Shechtman *et al* 1984) has generated a renewal of interest in the possible occurrence of icosahedral order in liquid alloys. Frank (1952) was the first to suggest that the structure of liquid metals could be based on icosahedral packing, in order to explain supercooling effects. Thirty years later, this description has been confirmed by molecular dynamics simulation of supercooled liquids (Steinhardt *et al* 1983). During the last few years, we have focused attention on the study of topological and chemical short-range order in $Al_{80}Mn_{20}$ and $Al_{80}Ni_{20}$ liquid alloys (Maret *et al* 1989, 1990), through the accurate determination of the partial pair correlation functions by neutron diffraction, using either isomorphous substitution (between Mn atoms and the σ-FeCr mixture) or Ni isotopic substitution. The first distances in both Al–Al and M–M distributions (M: transition metal atom) differ significantly in the two alloys, pointing out distinct topological ordering, the ordering extending to large distances in $Al_{80}Mn_{20}$ and being short range in $Al_{80}Ni_{20}$. This feature is emphasized in reciprocal space by the height difference observed for the first peak of

0953-8984/91/162801 + 17 $03.50

the number–number structure factor $S_{NN}(q)$ in the Bhatia–Thornton formalism (Bhatia and Thornton 1970). It is worthwhile to point out that, in the crystalline state, Al–Ni compounds are characterized by rather small unit cells whereas Al–Mn compounds have giant unit cells due to the formation of large size clusters of atoms.

In the first part of this paper we will ask ourselves two questions: do the S_{NN} functions of quasicrystal-forming liquids give evidence of local icosahedral order, and are there, as in many amorphous alloys, strong similarities between the local orders of the liquid phases and those of the corresponding crystalline alloys? For this purpose, three $Al_{1-x}Mn_x$ liquid alloys were investigated: two of them ($x = 0.14$, 0.267) being in the quasicrystal-forming range and one ($x = 0.4$) outside it (Murray *et al* 1987). Our data on $Al_{80}Mn_{20}$ liquid measured in a previous study will be reported as well. Moreover, for each composition there exists a compound of known structure: orthorhombic Al_6Mn, hexagonal μ-Al_4Mn, triclinic $Al_{11}Mn_4$ and rhombohedral γ-Al_8Cr_5. The S_{NN} functions will be directly obtained from neutron scattering experiments with alloys in which the transition metal mixture M, namely $Mn_{0.304}(Fe_{0.5}Cr_{0.5})_{0.696}$, has an average scattering length b_M equal to that of Al ($b_{Al} = 0.3449 \times 10^{-12}$ cm). The isomorphism between Mn atoms and the FeCr mixture was checked previously in the quasicrystalline (Janot *et al* 1986) as well as in the liquid state (Maret *et al* 1989). The comparison between the local order of the crystalline phase and that of the liquid is made with the help of a pseudo-crystalline model initially developed for the fluoride glasses (Le Bail *et al* 1985).

In the second part we give a detailed description of the local order for liquid $Al_{60}M_{40}$ as obtained from the determination of the three partial pair-correlation functions. These partials were extracted from three neutron-scattering measurements in liquid $Al_{60}M_{40}$ alloys with the following compositions: $Al_{60}Mn_{40}$, $Al_{60}(Mn_{0.639}(FeCr)_{0.361})_{40}$, and $Al_{60}(FeCr)_{40}$. In the second of these alloys the transition metal mixture has an average coherent scattering length equal to zero. Therefore, it yields information directly about the AlAl distribution. The local arrangement of atoms in $Al_{60}M_{40}$, as described by distances to nearest neighbours and coordination numbers, will then be compared with that previously determined in the quasicrystal-forming liquid $Al_{80}M_{20}$ (Maret *et al* 1989).

2. Experimental technique

The neutron scattering measurements were carried out on the D4B diffractometer at the Institut Laue Langevin (Grenoble) using a wavelength of 0.704 Å, with the same experimental conditions (sapphire cells, vanadium furnace) as for liquid $Al_{80}M_{20}$. The measurements were carried out at temperatures 30 to 40 K higher than the liquidus line (table 1). The influence of temperature on the structure was investigated for $Al_{86}M_{14}$ by measuring the $S_{NN}(q)$ function at 30 and 200 K above T_m. The momentum transfer range covered was from 0.28 to 16.4 $Å^{-1}$. However, since the sapphire container correction was not satisfactory at high q values, the results will only be shown up to 14 $Å^{-1}$.

The corrections applied to the raw data in order to determine the total structure factor are described elsewhere (Maret *et al* 1989). The isomorphous behaviour between Mn atoms and the σ-FeCr mixture allows us to consider the liquid alloys $Al_{1-x}(Mn_y(FeCr)_{1-y})_x$ as pseudo-binary alloys $Al_{1-x}M_x$. This description requires one to subtract from the total scattering intensity an incoherent scattering term arising from the random mixing of the isomorphous components (as shown in the appendix). In table 1 we have summarized the main input and output parameters of the data analysis. The

atomic densities ρ were estimated from the density measurements of liquid AlFe and AlCr (Levin and Ayushina 1974). The long-wavelength limits $S(0)$ were obtained from the thermodynamic properties of the alloys as follows:

$$S(0) = (\langle b\rangle^2/\langle b^2\rangle)\rho k_B T K_T + [(\langle b\rangle\delta - \Delta b)^2/\langle b^2\rangle]c_{Al}c_M S_{CC}(0) \qquad (1)$$

where,

$$\langle b\rangle = \sum_{i=M,Al} c_i b_i \qquad \langle b^2\rangle = \sum_{i=M,Al} c_i b_i^2 \qquad \Delta b = b_M - b_{Al}.$$

Table 1. Measuring temperatures, atomic densities, thermodynamic limits, values of the structure factor measured at 0.28 Å^{-1} and effective Bohr magneton number per M atom (M = Mn, σ-FeCr) for the $Al_{1-x}(Mn_y(FeCr)_{1-y})_x$ liquid alloys.

	T(K)	ρ (at Å^{-3})	$S_{CC}(0)$	$S(0)$	$S_m(0.28)$	μ_{eff}
$Al_{86}(Mn_{0.304}(FeCr)_{0.696})_{14}$	1335	0.054	0.424	0.038	0.32	2.2
$Al_{86}(Mn_{0.304}(FeCr)_{0.696})_{14}$	1510	0.052	0.466	0.04	0.37	2.4
$Al_{80}(Mn_{0.304}(FeCr)_{0.696})_{20}$	1395	0.058	0.365	0.042	0.505	2.4
$Al_{73.3}(Mn_{0.304}(FeCr)_{0.696})_{26.7}$	1430	0.059	0.356	0.044	0.404	1.8
$Al_{60}(Mn_{0.304}(FeCr)_{0.696})_{40}$	1505	0.064	0.355	0.055	0.82	2.2
$Al_{60}Mn_{40}$	1470	0.064	0.355	0.314	1.82	3.2
$Al_{60}(Mn_{0.639}(FeCr)_{0.361})_{40}$	1500	0.064	0.355	0.086	2.06	2.7
$Al_{60}(FeCr)_{40}$	1545	0.064	0.355	0.144	0.41	1.9

The values of $S_{CC}(0)$ (table 1) are calculated from the analytical expression of the excess Gibbs energies of the liquid $Al_{1-x}Mn_x$ alloys given by Murray *et al* (1987). The values of the isothermal compressibility K_T of the liquids $Al_{1-x}Mn_x$ are deduced from sound velocity calculations (Tekuchev and Stremousov 1985). In (1) δ is an expansion factor defined by $\delta = (1/V)(\partial V/\partial c_M)_{T,P}$, V being the molar volume of the alloy. The value of the effective Bohr magneton number per M atom, μ_{eff}, given in table 1, is deduced from the difference between the thermodynamic limit $S(0)$ and the measured value of $S(q)$ at 0.28 Å^{-1} (see Maret *et al* 1989). For a given transition metal mixture, μ_{eff} varies weakly with the Al concentration. By contrast, in the series of the $Al_{60}M_{40}$ liquids, μ_{eff} increases strongly with Mn concentration, as already observed for the $Al_{80}M_{20}$ liquids.

3. Number–number structure factors of the liquid alloys $Al_{1-x}M_x$ ($x = 0.14$, 0.267 and 0.4)

The variation of $S_{NN}(q)$ as a function of the alloy composition is shown in figure 1. The functions $S_{NN}(q)$ determined previously for the liquids $Al_{80}M_{20}$ and $Al_{80}Ni_{20}$ are also drawn for comparison.

As x increases, the following trends can be pointed out:

(i) The position changes of the first and second peaks of $S_{NN}(q)$ are very small for x ranging from 0.14 to 0.267 and become more pronounced for 0.4, with a shift to higher q values (see table 2 where the second peak is described as a double peak as will be discussed later).

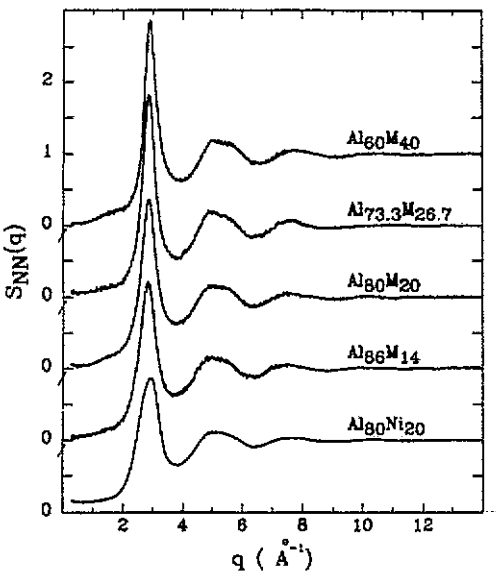

Figure 1. Number–number structure factor, $S_{NN}(q)$, for liquid $Al_{1-x}M_x$ ($x = 0.14$, 0.2, 0.267 and 0.4) and $Al_{80}Ni_{20}$ alloys.

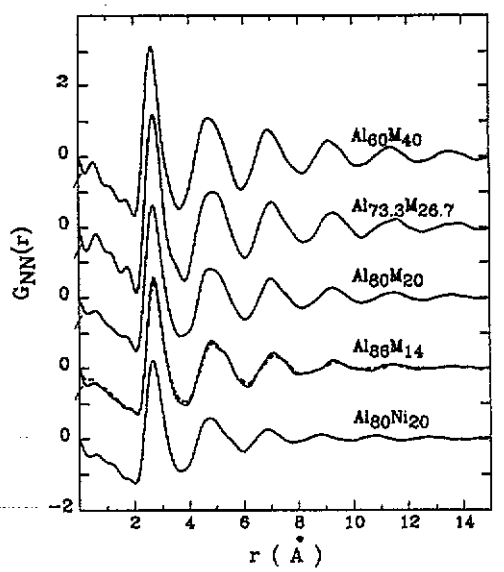

Figure 2. Number–number correlation function $G_{NN}(r)$ for liquid $Al_{1-x}M_x$ ($x = 0.14$, 0.2, 0.267 and 0.4) and $Al_{80}Ni_{20}$ alloys. For $x = 0.14$ the full curve was measured at 1335 K and the broken curve at 1510 K.

(ii) The strong increase of the first-peak height is undoubtedly the most striking feature, although the measurements were carried out at increasingly higher temperatures with x increasing.

The temperature effect has been studied for liquid $Al_{86}M_{14}$ by measuring $S_{NN}(q)$ at two temperatures. For an increase of 175 K, the first peak height decreases by 5%, while it increases by 30% for a temperature increase of 170 K between the extreme compositions.

An interesting feature observed in all the S_{NN} functions of $Al_{1-x}M_x$ is the existence of a hump around 1.6 Å^{-1}. This hump arises from correlations between second neighbours, which would yield a strong prepeak in the partial structure factor relative to the minority atom pairs, as observed in many amorphous alloys and recently in liquid $Al_{80}M_{20}$ and $Al_{80}Ni_{20}$. This prepeak has been connected by Moss and Price (1985) with the first sharp diffraction peak (FSDP) in the total structure factor of oxide and chalcogenide glasses or elemental semiconducting glasses, where it arises from the interconnectivity of basic structural units. Here, the diffuse prepeak in the $S_{NN}(q)$s of liquid $Al_{1-x}M_x$ suggests that structural units should exist but would be weakly correlated.

Figure 2 shows the number–number correlation functions obtained by Fourier transformation of $S_{NN}(q)$ as:

$$G_{NN}(r) = \frac{2}{\pi}\int_{q_{min}}^{q_{max}} q(S_{NN}(q) - 1)\sin qr\,dq \qquad (2)$$

with $q_{min} = 0.28$ Å^{-1} and q_{max} equal to 11.9, 10.6, 11.6 and 11 Å^{-1} for $x = 0.14, 0.2, 0.267$ and 0.4, respectively. We have checked that choosing a higher truncation value leads to similar curves but with more spurious ripples at high r values.

In table 2, we have reported the main characteristics of these functions. The average

Table 2. Peak positions in $Å^{-1}$ (or Å) and intensities (in parentheses) of the main peaks of the experimental functions, $S_{NN}(q)$ and $G_{NN}(r)$, for the liquid $Al_{1-x}M_x$ alloys. Correlation lengths ξ_{NN}(Å) for the topological order, coordination numbers in the first shell. Packing fraction, positions and intensities of the main peaks of $S_{NN}(q)$, and correlation length in the hard sphere model.

	Neutron scattering experiments							Hard sphere model			
Alloy composition	Temperature	First peak of $S_{NN}(q)$	Second peak of $S_{NN}(q)$		Correlation length ξ_{NN}	First peak of $G_{NN}(r)$	Coordination number	Packing fraction	First peak of $S_{NN}(q)$	Second peak of $S_{NN}(q)$	Correlation length ξ_{NN}
$Al_{86}M_{14}$	1335	2.85 (2.18)	~4.93 (1.13)	~5.45 (1.09)	9	2.71 (2.56)	11.1	0.40	2.72 (2.07)	5.17 (1.22)	6.9
$Al_{86}M_{14}$	1510	2.84 (2.07)	~4.95 (1.1)	~5.45 (1.08)	8.5	2.71 (2.39)	10.7	—	—	—	—
$Al_{80}M_{20}$	1395	2.86 (2.35)	~4.94 (1.14)	~5.46 (1.11)	10	2.69 (2.61)	11.7	0.42	2.75 (2.20)	5.2 (1.24)	8.3
$Al_{73.3}M_{26.7}$	1430	2.86 (2.79)	~4.95 (1.18)	~5.43 (1.12)	11.7	2.70 (3.17)	12.2	0.45	2.80 (2.49)	5.23 (1.29)	9.8
$Al_{60}M_{40}$	1505	2.89 (2.85)	~5.04 (1.17)	~5.54 (1.14)	12	2.62 (3.12)	12.6	0.45	2.82 (2.47)	5.27 (1.29)	9.2

first interatomic distance r_1 remains constant from $x = 0.14$ to 0.267 and decreases significantly for $x = 0.4$, while the first peak height of $G_{NN}(r)$ irregularly increases up to 0.267, then decreases slightly for 0.4. The determination of the three partial correlation functions for the liquid $Al_{60}M_{40}$, presented in the next section, will allow us to explain clearly the r_1 behaviour from the knowledge of the three first distances Al–Al, M–Al and M–M. Let us first attempt to discuss the changes observed in $S_{NN}(q)$ and $G_{NN}(r)$ by comparison with those obtained from a hard sphere (HS) model using the Percus–Yevick approximation.

3.1. Comparison with the HS model

The values of the hard sphere diameter σ and packing fraction η for each species are calculated from the entropies of pure Al and Mn liquids at their melting points (i.e. $\sigma_{Al} = 2.47$ Å, $\eta_{Al} = 0.42$ and $\sigma_{Mn} = 2.32$ Å, $\eta_{Mn} = 0.46$). The packing fraction of the liquid alloy is calculated following the relation $\eta = (c_1\eta_1V_1 + c_2\eta_2V_2)/V_M$, where V_i is the atomic volume of each species, and V_M that of the alloy. In order to reproduce, as well as possible, the experimental change in S_{NN}, V_M is deduced from the atomic density extracted from the slope of $G_{NN}(r)$ at $r \to 0$. In table 2, we have reported the positions and the heights of the first and second peaks of $S_{NN}(q)$ within the HS model for the four studied liquid alloys with their corresponding hard-sphere packing fraction. Looking in particular at the relative variations, the HS model yields a regular increase of q_1 from 14 to 40 at.% M and also an increase of $S_{NN}(q_1)$ up to 26.7 at.% M associated with the increase of the packing fraction. Between 26.7 and 40 at.%, $S_{NN}(q_1)$ remains almost constant, mainly due to the levelling of η.

The comparison between the experimental results and those of the HS models allow us to draw the following conclusions:

(i) Since the experimental q_1 values do not monotonically increase with M content, as in the HS model (due to a monotonic decrease of the average HS diameter), we expect a change of one or several nearest-neighbour distances between the pairs AlAl, AlM and MM across the series of studied liquid alloys.

(ii) The increase of $S_{NN}(q_1)$ with the transition metal concentration is largely due to the packing fraction increase, which increases the extent of the topological ordering in the liquid as shown in table 2 by the experimental or computed (HS model) values of the correlation length ξ_{NN}, (ξ_{NN} being estimated from the width of the first S_{NN} peak using the Scherrer particle-size broadening relation, $2\pi/\Delta q_{NN}$). The experimental values of ξ_{NN} indicate that the atoms are ordered over one more atomic shell in the liquids $Al_{1-x}M_x$ than in simple liquid metals which are rather well represented by the hard-sphere model.

3.2. Analysis of the height ratio between the second and the first peak of $S_{NN}(q)$

No significant change in the shape of the second peak of $S_{NN}(q)$ is observed between the quasicrystal-forming liquid alloys and the alloy $Al_{60}M_{40}$. Indeed, the splitting of the second peak at positions equal to $1.7\,q_1$ and $2\,q_1$, suggestive of local icosahedral order (Sachdev and Nelson 1985) would be even more pronounced for the latter alloy. However, there is a large difference between the first peak heights of the series $Al_{1-x}M_x$ and that of the alloy $Al_{80}Ni_{20}$ (figure 1), and the second peak of $S_{NN}(q)$ always exhibits a rather flat top (extending from $1.7\,q_1$ to $2\,q_1$) in comparison with the rounded shape found for $Al_{80}Ni_{20}$. Despite the absence of a clear second-peak splitting, it is, nonetheless, worth studying the height ratio between the second and the first peak in detail. In table

Table 3. Experimental peak intensity ratios for different liquid and amorphous alloys and calculated values in the icosahedral and polytetrahedral models (Y: existence of second peak splitting, N: no splitting, I: second peak with a rather flat top extending from 1.7 q_1 to 2 q_1).

	Alloy composition	$S_{NN}(q_1)$	$S_{NN}(q_2^a)/S_{NN}(q_1)$	$S_{NN}(q_2^b)/S_{NN}(q_1)$	Splitting	Reference
Liquids	l-$Al_{86}M_{14}$ ($T = 1335$ K)	2.18	0.52	—	I	This work
	l-$Al_{86}M_{14}$ ($T = 1510$ K)	2.07	0.53	—	I	This work
	l-$Al_{80}M_{20}$	2.35	0.49	—	I	Maret *et al* 1989
	l-$Al_{73.3}M_{26.7}$	2.79	0.42	—	I	This work
	l-$Al_{60}M_{40}$	2.85	0.41	—	I	This work
	l-$Al_{80}Ni_{20}$	1.86	0.6	—	N	Maret *et al* 1990
	l-$Cu_{66}Ti_{34}$	2.31	0.58	—	N	He Fenglai *et al* 1986
	l-$Fe_{83}B_{17}$	2.73	0.43	0.38	Y	Nold *et al* 1983
	l-$Li_{50}Pb_{50}$	2.17	0.57	—	N	Ruppersberg and Reiter 1982
	l-$Mg_{73}Zn_{27}$	2.64	0.47	—	I	Bühler *et al* 1987
Amorphous	a-$Al_{72}Mn_{22}Si_6$	2.61	0.49	0.47	Y	Robertson *et al* 1988
	a-$Fe_{80}B_{20}$	3.21	0.38	0.33	Y	Nold *et al* 1981
	a-$Mg_{72}Zn_{28}$	3.5	0.45	0.32	Y	Andonov and Chieux 1987
	a-$Ni_{33}Y_{67}$	2.27	0.55	—	N	Maret *et al* 1987
	a-$Ni_{40}Ti_{60}$	3.36	0.41	0.33	Y	Fukunuga *et al* 1984
	a-$Ni_{64}Zr_{36}$	3.02	0.46	0.39	Y	Lefebvre *et al* 1985
	a-$Ni_{81}B_{19}$	3.03	0.42	0.32	Y	Lamparter *et al* 1982
Models	Landau description of short-range icosahedral order	3.7	0.49 ($q_2^a = 1.706\, q_1$)	0.37 ($q_2^b = 2.04\, q_1$)	Y	Sachdev and Nelson 1984
	Regular polytetrahedral network	2.32	0.62 ($q_2^a = 1.71\, q_1$)	0.52 ($q_2^b = 1.97\, q_1$)	Y	Bletry 1980

3, we present these ratios for the $Al_{1-x}M_x$ liquid alloys as well as for other liquid or amorphous alloys. For a few alloys the function $S_{NN}(q)$ was not measured, and the ratio refers to the total structure factor (neutron or x-ray) in which, in any case, the contribution of $S_{NN}(q)$ is higher than 90%. When the second peak is not clearly split (case I in table 3), the height of its maximum near $1.7\,q_1$ is taken for the calculation of the ratio. For comparison we have also indicated the values of $S(q_2^a)/S(q_1)$ and $S(q_2^b)/S(q_1)$ using a Landau description of short-range icosahedral order ($q_2^a = 1.706\,q_1$ and $q_2^b = 2.04\,q_1$, Sachdev and Nelson 1984), and those obtained in the case of a regular polytetrahedral network, corresponding to a packing fraction of 0.437 (i.e. near that of liquid $Al_{1-x}M_x$ alloys). We note that in this last model a splitting of the second peak at positions $1.71\,q_1$ and $1.97\,q_1$ is observed (Bletry 1980), i.e. very close to those suggestive of icosahedral order. In fact, the two types of order differ only through the values of their peak intensity ratios (see table 3).

For all the amorphous alloys quoted in table 3, which exhibit a splitting of the second peak at positions around $1.7\,q_1$ and $2\,q_1$, the experimental peak-intensity ratios, $S_{NN}(q_2^a)/S_{NN}(q_1)$ are equal or smaller than that associated with a short-range icosahedral order. In particular, for the amorphous film of $Al_{72}M_{22}Si_6$ (a quasicrystal forming alloy), $S_{NN}(q_2^a)/S_{NN}(q_1)$ is exactly equal to the value of the icosahedral model. The amorphous alloys quoted in the present list were chosen in such a way as to emphasize that many metallic glasses may depart significantly from the expectation of Sachdev and Nelson (1984, 1985). The icosahedral order, therefore, does not seem to prevail in all amorphous metals (but it obviously occurs in some of them as, e.g. a-$Al_{72}Mn_{22}Si_6$) in accordance with structural models based on packings of trigonal prisms dedicated to a-$Ni_{81}B_{19}$ (Dubois *et al* 1985) or a-$Ni_{33}Y_{67}$ (Dubois 1985). Among the liquid alloys we can distinguish those exhibiting a shoulder on the right hand side of the second peak rather than a splitting (denoted by I in table 3) from those without any splitting. In the first category, the liquid $Al_{80}M_{20}$, shows a ratio exactly equal to 0.49 which is suggestive of icosahedral order. (We find significant that this specific ratio is obtained at exactly the quasicrystal composition. Note also that some shift from this ratio is observed for the $Al_{1-x}M_x$ liquids with different compositions.) The ratios found for the liquids: $Al_{80}Ni_{20}$, $Cu_{66}Ti_{34}$ and $Li_{50}Pb_{50}$, belonging to the second category, are closer to 0.62 and representative of tetrahedral order. The rapid fall off of the Bragg peak intensities of the icosahedral crystal has been predicted by a density-functional mean-field theory (Sachdev and Nelson 1985). Consequently, a rapid decrease between the first and the second peak of the topological order function seems to be a prerequisite of the existence of a local icosahedral order in liquid and amorphous alloys. Furthermore, we may already conclude from table 3 that icosahedral ordering preexists in $Al_{1-x}M_x$ liquid alloys with a definite enhancement around the 80/20 composition.

3.3. Modelling the S_{NN} function of liquids $Al_{1-x}M_x$ using a pseudocrystalline model

The idea that icosahedral order could preexist in the liquids $Al_{1-x}M_x$ is also supported by the relatively good representation of the S_{NN} functions up to the second peak (figure 3), using a pseudocrystalline model (Le Bail *et al* 1985) in which the initial structure is the one of the α-AlMnSi phase (Cooper and Robinson 1966). Elser and Henley (1985) have shown that this phase can be described as a packing of 54-atom Mackay icosahedra (MI) and is closely related to the icosahedral AlMnSi alloys (see also Guyot and Audier 1985). In order to represent the S_{NN} functions of liquids, the diffraction lines of the initial solid phase were broadened by a Gaussian strain distribution. The calculated S_{NN}

functions could then be obtained from a scattering angle of 4° to one of 100° after a refinement of the cubic cell parameter a_0 and of 21 atomic positions, using the principles of the Rietveld pattern fitting technique (Rietveld 1969). Starting from the α-AlMnSi structure, all the calculated functions (full curves in figure 3) exhibit a shoulder on the right hand side of the second peak and a diffuse prepeak (~10°) in good agreement with the experiments. For each composition, other modellings have been attempted, starting from the structure of the corresponding crystalline alloys: the orthorhombic Al_6Mn (Nicol 1953), the hexagonal μ-Al_4Mn (Brink-Shoemaker *et al* 1989) the triclinic δ-$Al_{11}Mn_4$ (Bland 1958) and the rhombohedral γ-Cr_5Al_8 (Brandon *et al* 1977). Save the γ-phase, it is interesting to note that in Al_6Mn and $Al_{11}Mn_4$ Mn atoms have coordination groups of Al atoms forming nearly icosahedral clusters and in μ-Al_4Mn fragments of MI are present. As can be observed in figure 3, the diffuse prepeak and the shoulder of the second peak of the experimental functions $S_{NN}(q)$ are not as well described from these initial structures (broken curves in figure 3(*a*), (*c*) and (*d*)). For the $Al_{80}M_{20}$ alloy, a complete refinement of all parameters in the μ-phase was impossible to achieve due to the very large number of atomic sites. However, if the refinement is restricted to the cell parameters, scaling factor and strain parameter, the calculated curve obtained from the μ-phase is similar to that obtained from the α-phase with the same parameters (see figure 3(*b*)). The curves calculated from the μ-Al_4Mn and γ-Cr_5Al_8 phase fall off above 50° (2θ) because the number of reflections to be handled for these structures exceeds the size limit of the model, therefore they are not shown above this value. In the next section, we will see other reasons why a good representation of the S_{NN} second peak cannot be obtained from the γ-phase.

In conclusion, no significant change has been observed between the functions $S_{NN}(q)$ of the quasicrystal-forming liquids and that of the liquid $Al_{60}M_{40}$. The values of the intensity ratio $S_{NN}(q_2^a)/S_{NN}(q_1)$ found in the four liquid alloys $Al_{1-x}M_x$ are close to the value expected for an icosahedral crystal and suggest the preexistence of a local icosahedral order in the liquid phases. This idea is supported by the good representation of the experimental functions using a pseudo-crystalline model starting from the α-AlMnSi structure (closely related to that of the icosahedral AlMnSi alloy) and in which the atomic sites can be occupied indistinctively by Al or Mn atoms. In the next section, the determination of the three pair partial correlation functions for the alloy $Al_{60}M_{40}$ will allow us to see how each atomic pair contributes to the decrease of the mean interatomic distance shown in $G_{NN}(r)$ as the transition metal concentration increases.

4. Determination of the structure of the liquid $Al_{60}M_{40}$ alloy

4.1. Total structure factors

The partial structure factors (PSFs) of the liquid $Al_{60}M_{40}$ have been determined from the three total structure factors $S(q)$ of the liquid alloys $Al_{60}(Mn_y(FeCr)_{1-y})_{40}$ with $y = 1$, 0.639 and 0 (figure 4). In table 4, we have reported the weights of the Bathia–Thornton PSFs (Bhatia and Thornton 1970) and the Faber-Ziman PSFs (Faber and Ziman 1965) in the total functions defined by the following equations:

$$S(q) = (\langle b^2\rangle/\langle b^2\rangle)S_{NN}(q) + (2\Delta b\langle b\rangle/\langle b^2\rangle)S_{NC}(q) + (c_M c_{Al}(\Delta b)^2/\langle b^2\rangle)S_{CC}(q)$$
$$= \sum_{i,j=N,C} W_{ij}S_{ij}(q) \qquad (3)$$

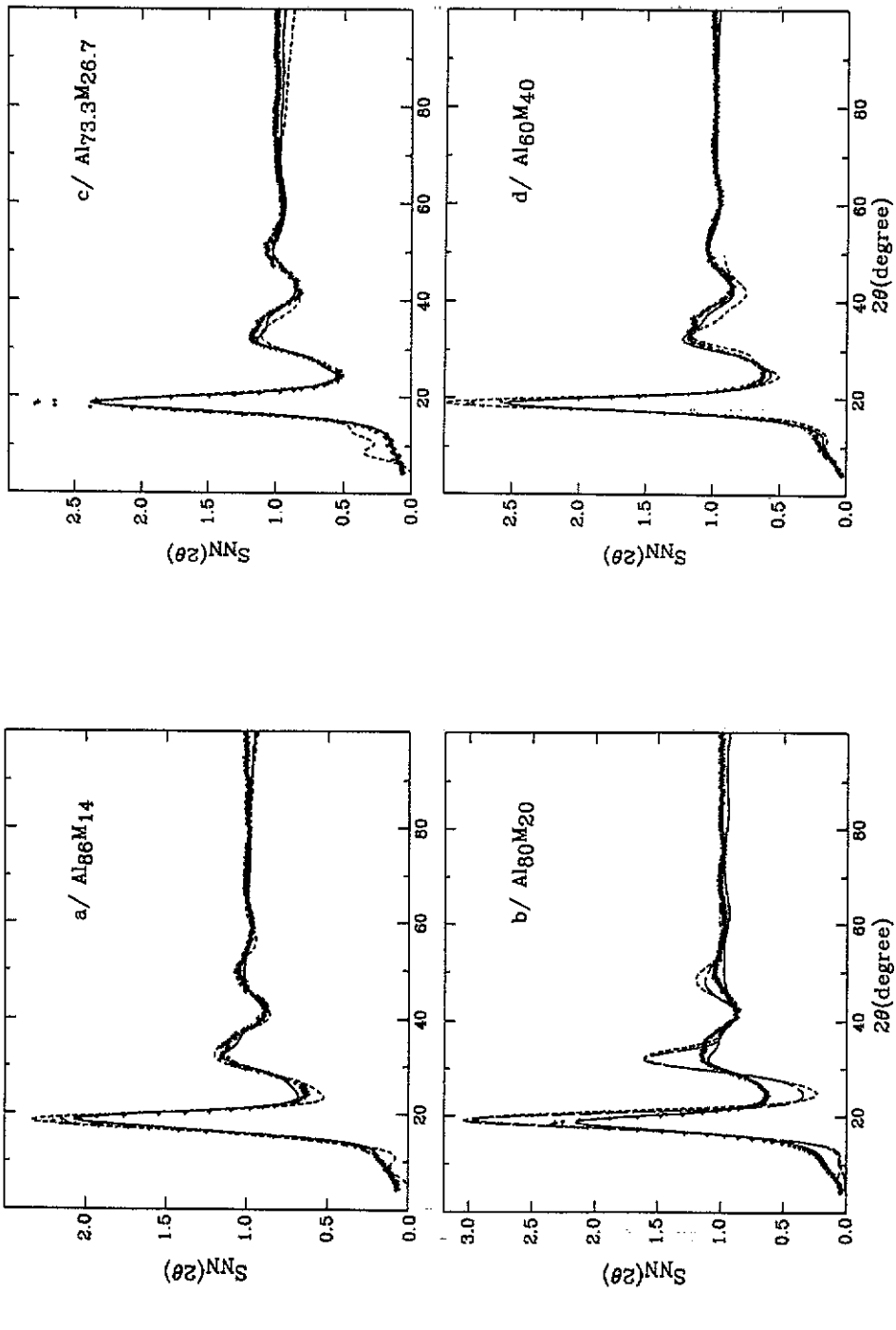

Figure 3. Comparison of the various experimental number–number structure factors of liquid $Al_{1-x}M_x$ (crosses) with those obtained from a pseudocrystalline model starting from the α-AlMnSi structures (full curves) or from the corresponding crystalline alloy structures (broken curves): (*a*) o-Al_6Mn, (*b*) μ-Al_4Mn, (*c*) δ-$Al_{11}Mn_4$, (*d*) γ-Cr_5Al_8. In (*b*), the short-dashed and long-dashed broken curves are obtained, respectively, from the μ and α structures after a refinement restricted to the cell parameters, the scaling factor and the strain parameter.

Table 4. Weighting factors of the partial structure factors defined in (3) and (4).

Alloy composition	W_{NN}	W_{NC}	W_{CC}	W_{MM}	W_{MAl}	W_{AlAl}
$Al_{60}(FeCr)_{40}$	0.903	1.206	0.097	0.314	0.493	0.193
$Al_{60}(Mn_{0.639}(FeCr)_{0.361})_{40}$	0.6	−2.0	0.4	0.0	0.0	1.0
$Al_{60}Mn_{40}$	0.026	−0.652	0.974	6.68	−18.52	12.84

and

$$I(q) = (c_M^2 b_M^2/\langle b\rangle^2)I_{MM}(q) + (c_{Al}^2 b_{Al}^2/\langle b\rangle^2)I_{AlAl}(q) + (2c_M c_{Al} b_M b_{Al}/\langle b^2\rangle)I_{MAl}(q)$$
$$= \sum_{i,j=M,Al} W_{ij} I_{ij}(q). \tag{4}$$

The two total functions $S(q)$ and $I(q)$ are related by:

$$(I(q) - 1)\langle b\rangle^2 = (S(q) - 1)\langle b^2\rangle.$$

As the Mn content increases, the first peak located at 2.9 $Å^{-1}$ attributed to the S_{NN} function, according to figure 1, decreases rapidly and disappears for $Al_{60}Mn_{40}$. In the meantime, a broad prepeak centred around 2 $Å^{-1}$ and originating from the chemical ordering function $S_{CC}(q)$, as shown below, emerges completely. Note also that the partial function $I_{AlAl}(q)$, which is directly proportional to the function $S(q)$ for $y = 0.639$, exhibits a well-marked shoulder on the left side of its first peak.

4.2. Partial structure factors

4.2.1. Bhatia–Thornton formalism. The Bhatia–Thornton PSFs (figure 5) are derived by solving the system of equations formed by the three measured $S(q)$s (3). The excellent

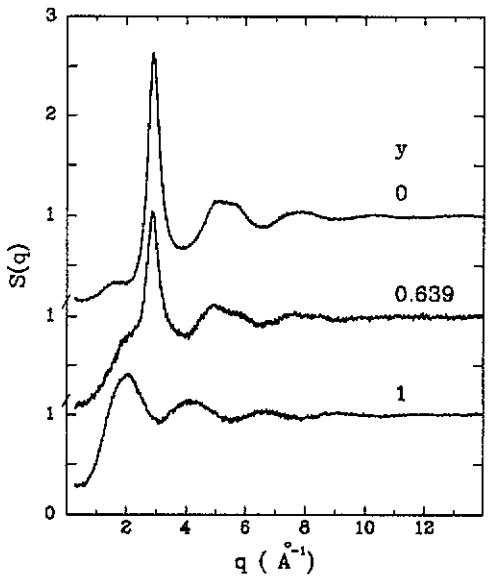

Figure 4. Total neutron structure factors of the liquid $Al_{60}(Mn_y(FeCr)_{1-y})_{40}$ alloys.

agreement between the derived S_{NN} function and the structure factor of the alloy $Al_{60}(Mn_{0.304}(FeCr)_{0.696})_{40}$ confirms well the isomorphism between the Mn atoms and the σ-FeCr mixture in Al-based alloys with up to 40% transition metal content, since, within statistical errors, no difference is detected between the two functions (other comments on $S_{NN}(q)$ have been given in section 3). The function $S_{CC}(q)$ is characterized by a broad first peak of relatively weak intensity centred at 2.02 $Å^{-1}$. Its width at half peak height yields a short-range chemical ordering correlation length of 4 Å (i.e. three times smaller than that of the topological ordering). The small amplitude of the first oscillation of $S_{NC}(q)$, about half of that measured for $Al_{80}M_{20}$, indicates that the atomic sizes of Al and M atoms are close in liquid $Al_{60}M_{40}$.

Figure 6 shows the three number–concentration correlation functions $G_{NN}(r)$, $G_{NC}(r)$ and $G_{CC}(r)$ in comparison with those measured for the liquid $Al_{80}M_{20}$ (Maret *et al* 1989). The oscillations of $G_{NN}(r)$, more pronounced for $Al_{60}M_{40}$, reveal the existence of atomic arrangements better defined at short and medium range.

4.2.2. Faber–Ziman formalism and the chemical short-range order parameter. The Faber–Ziman PSFs are determined from the three interference functions $I(q)$ (4) measured for $y = 0$, 0.639 and 1 (figure 7). All of them are characterized by superstructure effects, in particular, a well marked shoulder at 1.96 $Å^{-1}$ is visible on the left side of the first peak of $I_{AlAl}(q)$; the alloy composition close to the equiatomic composition favours this behaviour if chemical order effects exist (see for example, Lemarchand *et al* 1980). The first peak positions of the three $I_{ij}(q)$ are very close and equal to 2.91, 2.90 and 2.89 $Å^{-1}$ for the atomic pairs MM, MAl and AlAl, respectively.

The reduced partial pair-distribution functions $G_{ij}(r)$ of the liquid $Al_{60}M_{40}$, derived

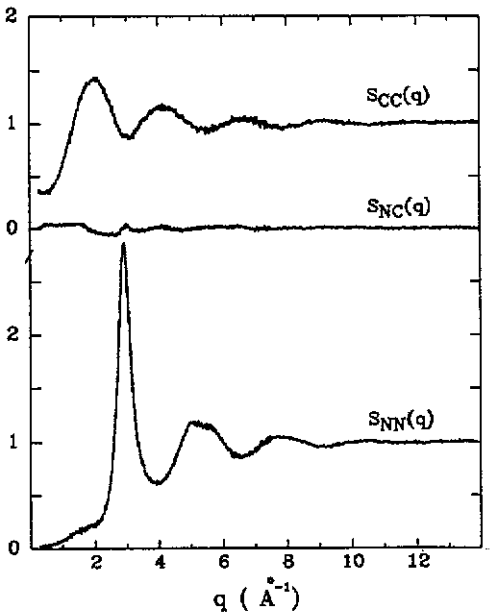

Figure 5. Bhatia–Thornton partial structure factors of liquid $Al_{60}(Mn_y(FeCr_{1-y})_{40}$ alloys.

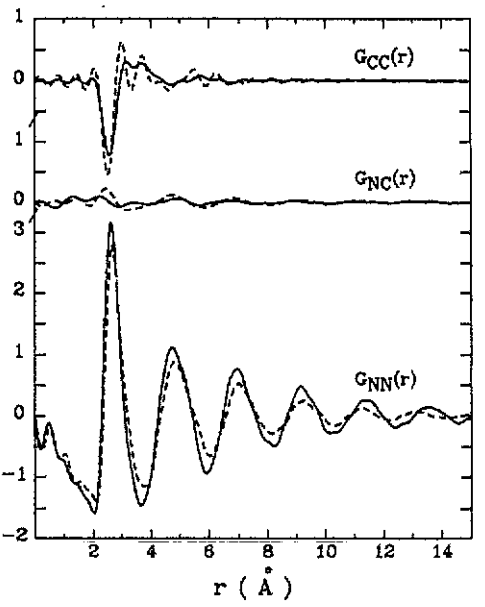

Figure 6. Number–concentration correlation functions for liquid $Al_{60}M_{40}$ (full curve) and $Al_{80}M_{20}$ (broken curve) alloys; M = Mn or σ-FeCr.

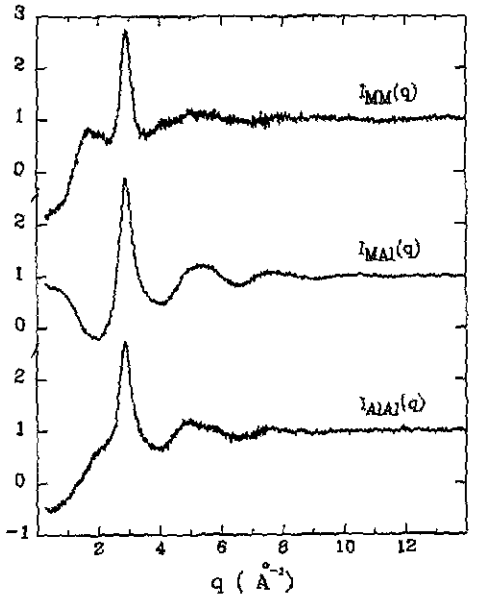

Figure 7. Faber–Ziman partial structure factors of liquid $Al_{60}(Mn_y(FeCr)_{1-y})_{40}$ alloys; M = Mn or σ-FeCr.

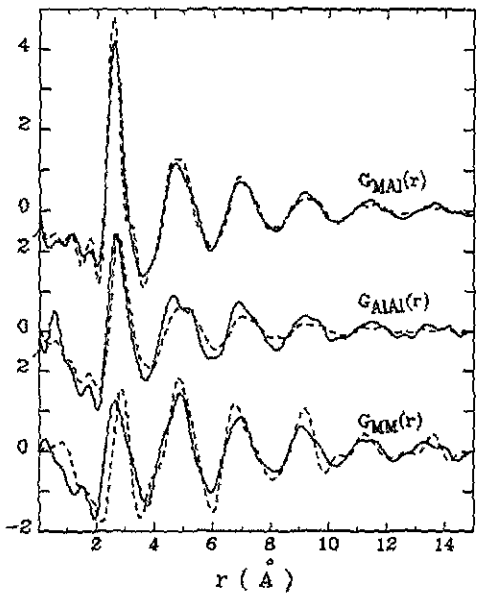

Figure 8. Reduced partial pair-correlation functions for liquid $Al_{60}Mn_{40}$ (full curve) and $Al_{80}M_{20}$ (broken curve) alloys; M = Mn or σ-FeCr.

from $I_{ij}(q)$, are shown in figure 8 with those corresponding to the liquid $Al_{80}M_{20}$. The two MAl distributions are exactly in phase indicating that the strength of heteroatomic interactions associated with the sp–d hybridization is independent of the liquid-alloy composition. By contrast, the MM first pair distributions are different, since for $Al_{60}M_{40}$ the first peak of $G_{MM}(r)$ shifts to smaller r values and becomes more asymmetrical and the MM distribution at higher distances is less well defined. The comparison of AlAl distributions shows a small shortening of the first distances and the existence of two components in the second pair distribution better resolved for $Al_{60}M_{40}$.

In table 5, the first and second interatomic distances (taken from the peak positions of the partial pair correlation functions: $g_{ij}(r) = G_{ij}(r)/4\pi\rho r + 1$) are reported for both

Table 5. Interatomic distances and coordination numbers in the liquid $Al_{60}(Mn_y(FeCr)_{1-y})_{40}$ and $Al_{80}(Mn_y(FeCr)_{1-y})_{20}$ alloys.

	Liquid $Al_{60}(Mn_y(FeCr)_{1-y})_{40}$		Liquid $Al_{80}(Mn_y(FeCr)_{1-y})_{20}$	
Atomic pair	r_{ij} (Å)	z_{ij}	r_{ij} (Å)	z_{ij}
M–M	2.61	4.5	2.89	1.5
	4.87	17.5	4.85	8.5
M–Al	2.59	7.8	2.56	9.5
	4.73	25	4.6, 4.9	31.8
Al–Al	2.65	7.4	2.74	10.2
	4.60, 5.2	26	4.8, ~5.3	32.7

alloys with the corresponding partial coordination numbers calculated as follows:

$$z_{ij}^{1} = c_j \int_{r_{ij,\min}^{1}}^{r_{ij,\max}^{1}} \varphi_{\mathrm{RDF}_{ij}}(r)\,\mathrm{d}r \tag{5}$$

with $\varphi_{\mathrm{RDF}_{ij}}(r) = rG_{ij}(r) + 4\pi r^2\rho$. In integral (5), $r_{ij,\min}^{1}$ and $r_{ij,\max}^{1}$ are the lower and upper limits of the first coordination shell given by the minima in $\varphi_{\mathrm{RDF}_{ij}}(r)$.

The nearest-neighbour distances for the three types of pairs are closer to each other in $Al_{60}M_{40}$ than in $Al_{80}M_{20}$. This result is in agreement with the difference in position between the first peak of $G_{\mathrm{NN}}(r)$ and the negative peak of $G_{\mathrm{CC}}(r)$, smaller for $Al_{60}M_{40}$ than for $Al_{80}M_{20}$, and is also in agreement with the reduction of the first significant oscillation of $G_{\mathrm{NC}}(r)$ around 2.8 Å for $Al_{60}M_{40}$ (see figure 6).

The most salient features are the shortening of the first MM interatomic distances in $Al_{60}M_{40}$ and the less pronounced shortening of the first AlAl distances, both being weakly compensated by the increase of the first MAl ones. Thus, the first MM distance in $Al_{60}M_{40}$ becomes comparable to the average value of pure liquid metals (2.68 Å for Mn and 2.58 Å for Cr or Fe, Waseda 1976), while the first AlAl distance departs still more from the value of 2.82 Å measured in liquid Al. The second AlAl distances are also shorter in $Al_{60}M_{40}$, while the second MAl and MM distances are similar in both alloys. The strength of chemical interactions is comparable in both alloys, as shown by the closeness of the first MAl distances. This is confirmed by the calculation of the Warren chemical short-range order parameter generalized by Wagner and Ruppersberg (1981) and defined by:

$$\alpha_1 = 1 - z_{\mathrm{MAl}}^{1}/c_{\mathrm{Al}}(c_{\mathrm{M}}z_{\mathrm{Al}}^{1} + c_{\mathrm{Al}}z_{\mathrm{M}}^{1})$$

with $z_i^1 = z_{ii}^1 + z_{ij}^1$, which yields a value of -0.045 for $Al_{60}M_{40}$ and is, therefore, very close to the -0.05 previously found for $Al_{80}M_{20}$†. Using the same first-coordination shell upper limit (defined as the first-minimum position of G_{NN} at 3.65 Å) for the calculation of the three partial coordination numbers z_{ij}^1 in integral (5), α_1 is equal to -0.07 (with $z_{\mathrm{MM}}^1 = 4.3$, $z_{\mathrm{MAl}}^1 = 7.9$ and $z_{\mathrm{AlAl}}^1 = 7.2$) and remains close to the value of -0.06 calculated for $Al_{80}M_{20}$ using the same restriction.

4.3. Comparison of the liquid structure with that of the corresponding crystalline alloy, γ-Cr_5Al_8

The first distances found in liquid $Al_{60}M_{40}$ are very far from the average distances calculated in the rhombohedral γ-Cr_5Al_8 structure, which are equal to 2.68 Å, 2.7 Å and 2.95 Å for the pairs CrCr, CrAl and AlAl, respectively (Brandon *et al* 1977). The structure of γ-Cr_5Al_8 can be considered as being built of clusters of 26 atoms, formed by an inner tetrahedron of four atoms surrounded by an outer tetrahedron, then an octahedron of six atoms followed, finally, by a cubo-octahedron of twelve atoms. Hence, the failure of the $S_{\mathrm{NN}}(q)$ representation based on the γ-Cr_5Al_8 structure in the pseudocrystalline model (see figure 3(*d*), broken curve) can be attributed to the differences in the interatomic distances and also to discrepancies in the symmetry of the

† The CSRO parameter values, $\alpha_1^0 = \alpha_1/\alpha_1^{\max}$, normalized with regard to a maximum order parameter $\alpha_1^{\max}$ obtained with $z_{\mathrm{MAl}}^1 = z_{\mathrm{M}}^1$ are equal to 0.07 for $Al_{60}M_{40}$ (with $\alpha_1^{\max} = -0.66$) and 0.23 for $Al_{80}M_{20}$ (with $\alpha_1^{\max} = -0.22$). However, when $c_{\mathrm{Al}} \sim c_{\mathrm{M}}$, the values of $\alpha_1^{\max}$ are ill-defined and possibly too high by as much as a factor of three (see Cargill and Spaepen 1981), consequently, by dividing $\alpha_1^{\max}$ by three for $Al_{60}M_{40}$, the normalized values α_1^0 are also comparable in both alloys.

atomic environments, since from the discussion in section 3, there is some indication of icosahedral order in the liquid phase $Al_{60}M_{40}$, while the γ structure exhibits no coordination group of atoms related to the icosahedron.

5. Conclusion

From this new series of neutron-scattering measurements in liquid Al_xM_{1-x}, (M = Mn or σ-FeCr), it is still difficult to draw firm conclusions in favour of local icosahedral order in liquid alloys above the melting point. However, the results presented in this paper together with those previously found for $Al_{80}M_{20}$ and $Al_{80}Ni_{20}$ have allowed us to point out clues that indicate icosahedral order in the S_{NN} functions of liquids Al_xM_{1-x}, which are absent for liquid $Al_{80}Ni_{20}$, which forms no quasicrystal; these are the existence of a sharp first peak, the height ratio between the two first peaks close to the value obtained from a Landau description of short-range icosahedral order, and the shape of the second peak that tends to form a double-component peak at positions $1.7\,q_1$ and $2\,q_1$.

Despite the fact that the alloy composition $Al_{60}M_{40}$ falls outside the quasicrystal-forming composition range, this alloy also exhibits a tendency towards icosahedral ordering. The differences between the local structures of the liquid $Al_{60}M_{40}$ and the corresponding crystalline alloy γ-Cr_5Al_8 (characterized by the absence of coordination groups related to the icosahedron) support this type of local order.

The comparison between the $Al_{80}M_{20}$ and $Al_{60}M_{40}$ liquids has shown that the strength of the heteroatomic interactions is similar in both alloys and that, by contrast, the local arrangements between homoatomic pairs change significantly with the transition metal concentration, as indicated by the shortening of the MM and AlAl first distances in $Al_{60}M_{40}$.

Acknowledgments

Allocation of beam time by the Institut Laue Langevin is gratefully acknowledged. We thank J P Houin for preparing the master ingots and Dr Le Bail for providing the program for modelling $S_{NN}(q)$.

Appendix

The Bhatia–Thornton formalism has been extended to multicomponent systems simultaneously by Bletry (1976) and Bhatia and Ratti (1977). The coherent scattering cross section per atom of systems containing ν species can be expressed by $\frac{1}{2}\nu\,(\nu+1)$ independent Bhatia–Thornton partial structure factors (Bletry 1979):

$$\frac{d\sigma_{coh}}{d\Omega}(q) = \langle b\rangle^2 S_{NN}(q) + 2\langle b\rangle \sum_i b_i c_i S_{NC_i}(q) + \tfrac{1}{2}\sum_{i,j} c_i c_j (b_i - b_j)^2 S_{C_iC_j}(q) \qquad \text{(A1)}$$

with $\langle b\rangle = \Sigma_i\, c_i b_i$, $\Sigma_i\, c_i = 1$, and $S_{C_iC_j}(q) = S_{C_jC_i}(q)$, $(i, j, = 1, 2, \ldots, \nu)$.

The PSFs obey the sum rules:

$$\sum_i c_i S_{NC_i}(q) = 0 \qquad \sum_j c_j S_{C_iC_j}(q) = 0$$

and are related to the $\frac{1}{2}\nu(\nu+1)$ Faber–Ziman PSFs by:

$$S_{NN}(q) = \sum_{i,j} c_i c_j a_{ij}(q)$$

$$S_{NC_i}(q) = \sum_{j} c_j a_{ij}(q) - \sum_{k,l} c_k c_l a_{kl}(q) \tag{A2}$$

$$S_{C_iC_j}(q) = 1 - \delta_{ij}/c_i - a_{ij}(q) + \sum_{k} c_k(a_{ik}(q) + a_{jk}(q)) - \sum_{k,l} c_k c_l a_{kl}(q).$$

If the species $2, 3, \ldots, \nu$ are isomorphous, the functions $a_{1j}(q)$ with $j = 2, 3, \ldots, \nu$ are all equal and the functions $a_{kl}(q)$ $(k, l = 2, 3, \ldots, \nu)$ are also identical. Indeed, the $a_{ij}(q)$ are defined by:

$$a_{ij}(q) = 1 + \rho \int (g_{ij}(r) - 1)\, e^{iqr}\, d^3r$$

and only depend on the pair probabilities ($g_{ij}(r)$ normalized to 1 at large r values). Therefore, the $g_{kl}(r)$ are the same for any pair of isomorphous elements (the atomic concentrations being taken into consideration for the calculation of the partial coordination numbers only). The $g_{1j}(r)$ are also identical.

Using these equalities in relations (A2) we find the following relations between the multicomponent $(1, 2, \ldots, \nu)$ and the pseudo-binary (1, M) Bhatia–Thornton PSFs.

$$S_{NC_2}(q) = S_{NC_3}(q) = \ldots = S_{NC_\nu}(q) = S_{NC_M}(q)$$

$$S_{C_1C_2}(q) = S_{C_1C_3}(q) = \ldots = S_{C_1C_\nu}(q) = S_{C_1C_M}(q)$$

and

$$S_{C_iC_j}(q) = (1/c_M)(1 - c_1 S_{C_1C_M}) \qquad (i, j = 2, \ldots, \nu)$$

$$c_M = \sum_{i} c_i \qquad (i = 2, \ldots, \nu).$$

Finally, the coherent scattering cross section of the pseudo-binary system (1, M) is simply given by:

$$\frac{d\sigma}{d\Omega}(q) = \langle b\rangle^2 S_{NN}(q) + 2\langle b\rangle(b_1 - b_M)c_1 S_{NC_1}(q)$$

$$+ c_1 c_M (b_1 - b_M)^2 S_{C_1C_M}(q) + \frac{1}{2}\sum_{i\neq j=2,\ldots,\nu} \frac{c_i c_j}{c_M}(b_i - b_j)^2 \tag{A3}$$

where $c_M b_M = \Sigma_i\, c_i b_i$, $(i = 2, \ldots, \nu)$ and $c_1 S_{NC_1}(q) = -c_M S_{NC_M}(q)$. The last term in (A3) represents the incoherent scattering due to the mixing of the isomorphous species and can be rewritten as:

$$\frac{1}{2}\sum \frac{c_i c_j}{c_M}(b_i - b_j)^2 = c_M\left(\sum_j \frac{c_j}{c_M} b_j^2 - b_M^2\right) \qquad i, j = 2, \ldots, \nu.$$

The functions $S_{NC}(q)$ and $S_{CC}(q)$ determined in section 4.2 are related to $S_{NC_1}(q)$ and $S_{C_1C_M}$ through:

$$S_{NC}(q) = -c_1 S_{NC_1}(q) \qquad S_{CC}(q) = S_{C_1C_M}(q)$$

References

Andonov P and Chieux P 1987 *J. Non-Cryst. Solids* **93** 331
Bhatia A B and Ratti V K 1977 *Phys. Chem. Liq.* **6** 201
Bhatia A B and Thornton D E 1970 *Phys. Rev.* B **2** 3004
Bland J A 1958 *Acta Crystallogr.* **11** 236
Bletry J 1976 *Z. Naturf.* a **31** 960
Bletry J 1979 *Thèse d'Etat* Grenoble University
Bletry J 1980 *Revue Phys. Appl.* **15** 1019
Brandon J K, Pearson W B, Riley P W, Chiech C and Stokhuyzen R 1977 *Acta Crystallogr.* B **33** 1088
Brink-Shoemaker C, Keszler D A and Schoemaker D P 1989 *Acta Crystallogr.* B **45** 13
Bühler E, Lamparter P and Steeb S 1987 *Z. Naturf.* a **42** 507
Cargill III G S and Spaepen F 1981 *J. Non-Cryst. Solids* **43** 91
Cooper M and Robinson K 1966 *Acta Crystallogr.* **20** 614
Dubois J M 1985 *J. Physique Coll.* **46** C8 335
Dubois J M, Gaskell P H and Le Caer G 1985 *Proc. Roy. Soc.* A **402** 323
Elser V and Henley C L 1985 *Phys. Rev. Lett.* **55** 2883
Faber T E and Ziman J M 1965 *Phil. Mag.* **11** 153
Frank F C 1952 *Proc. Roy. Soc.* A **215** 43
Fukunuga T, Watanabe N and Suzuki K 1984 *J. Non-Cryst. Solids* **61/62** 343
Guyot P and Audier M 1985 *Phil. Mag.* B **52** 45
He Fenglai F, Cowlam N, Carr G E and Suck J B 1986 *Phys. Chem. Liq.* **16** 99
Janot Ch, Pannetier J, Dubois J M and Fruchart R 1986 *Phys. Rev. Lett.* A **119** 309
Lamparter P, Sperl W, Steeb S and Bletry J 1982 *Z. Naturf.* a **37** 1223
Le Bail A, Jacoboni C and De Pape R 1985 *J. Physique Coll.* **46** C8 163
Lefebvre S, Quivy A, Bigot J, Calvayrac Y and Bellissent R 1985 *J. Phys. F: Met. Phys.* **15** L99
Lemarchand J L, Bletry J and Desre P 1980 *J. Physique Coll. France* **41** C8 163
Levin E S and Ayushina G D 1974 *Tr. Ural Politekn. Inst.* **231** 93
Maret M, Chieux P, Hicter P, Atzmon M and Johnson W L 1987 *J. Phys. F: Met. Phys.* **17** 315
Maret M, Pasturel A, Senillou C, Dubois J M and Chieux P 1989 *J. Physique.* **50** 295
Maret M, Pomme T, Pasturel A and Chieux P 1990 *Phys. Rev.* B **42** 1598
Moss S C and Price D L 1985 *Physics of Disordered Materials* ed D Adler, H Fritzshe and S R Ovshinsky (New York: Plenum) p 77
Murray J L, McAlister A J, Schaeffer R J, Bendersky L A, Biancaniello F S and Moffat D L 1987 *Metall. Trans.* A **18** 385
Nicol D I 1953 *Acta Crystallogr.* **6** 285
Nold E, Lamparter P, Olbrich H, Rainer-Harbach G and Steeb S 1981 *Z. Naturf.* a **36** 1032
Nold E, Rainer-Harbach G, Lamparter P and Steeb S 1983 *Z. Naturf.* a **38** 325
Rietveld H M 1969 *J. Appl. Crystallogr.* **2** 65
Robertson J L, Moss S C and Kreider K G 1988 *Phys. Rev. Lett.* **60** 2062
Ruppersberg H and Reiter H 1982 *J. Phys. F: Met. Phys.* **12** 1311
Sachdev S and Nelson D R 1984 *Phys. Rev. Lett.* **53** 1947
—— 1985 *Phys. Rev.* B **32** 4592
Shechtman D, Blech I, Gratias D and Cahn J W 1984 *Phys. Rev. Lett.* **53** 1951
Steinhardt P J, Nelson D R and Ronchetti M 1983 *Phys. Rev.* B **28** 784
Tekuchev V V and Stremousov V I 1985 *Zh. Fiz. Khim* **59** 2258
Wagner C N J and Ruppersberg H 1981 *Atomic Energy Review* **1** 101
Waseda Y 1976 *Liquid Metals (Inst. Phys. Conf. Ser. 30)* ed R Evans and D A Greenwood (Bristol: Institute of Physics) p 230